



Regenerated silk fibroin membranes as separators for transparent microbial fuel cells

Grzegorz Pasternak^{a,c,*}, Yuejiao Yang^b, Bruno Bosquiroli Santos^{a,d}, Federico Brunello^a, Martin M. Hanczyc^{a,e}, Antonella Motta^b

^a Laboratory for Artificial Biology, Centre for Integrative Biology, University of Trento, Polo Scientifico e Tecnologico Fabio Ferrari, Polo B, Via Sommarive 9, 38123 Povo TN, Italy

^b Department of Industrial Engineering and BIOTech Research Center, University of Trento, via Sommarive 9, 38123 Trento, Italy

^c Faculty of Chemistry, Wrocław University of Technology, Wyb. Wyspiańskiego 27, 50-370 Wrocław, Poland

^d Engineering School of Lorena, University of São Paulo, 12-602-810 Lorena, SP, Brazil

^e Chemical and Biological Engineering, University of New Mexico, USA

ARTICLE INFO

Article history:

Received 12 October 2018

Received in revised form 10 December 2018

Accepted 12 December 2018

Available online 17 December 2018

Keywords:

Membrane

Sustainable

Transparent

MFC

Bioelectrochemical system

Biopolymer

ABSTRACT

In recent years novel applications of bioelectrochemical systems are exemplified by phototrophic biocathodes, biocompatible enzymatic fuel cells and biodegradable microbial fuel cells (MFCs). Herein, transparent silk fibroin membranes (SFM) with various fibroin content (2%, 4% and 8%) were synthesised and employed as separators in MFCs and compared with standard cation exchange membranes (CEM) as a control. The highest real-time power performance of thin-film SFM was reached by 2%-SFM separators: $25.7 \pm 7.4 \mu\text{W}$, which corresponds to 68% of the performance of the CEM separators ($37.7 \pm 3.1 \mu\text{W}$). Similarly, 2%-SFM revealed the highest coulombic efficiency of $6.65 \pm 1.90\%$, 74% of the CEM efficiency. Current for 2%-SFM reached $0.25 \pm 0.03 \text{ mA}$ (86% of CEM control). Decrease of power output was observed after 23 days for 8% and 4% and was a consequence of deterioration of SFMs, determined by physical, chemical and biological studies. This is the first time that economical and transparent silk fibroin polymers were successfully employed in MFCs.

© 2018 The Authors. Published by Elsevier B.V. This is an open access article under the CC BY license (<http://creativecommons.org/licenses/by/4.0/>).

1. Introduction

Over the past decade, there has been expanding development of microbial fuel cells with the overall functionality of providing organic waste as input and generating electricity and other value added products as output. The MFC consists of an anode and cathode connected through conductive material to shuttle electrons as well as a semi-selective exchange membrane that allows passage of protons to complete the circuit. Design of the MFC systems spans various size scales from microliters to pilot-scale reactors demonstrating power densities that make this technology useful and applicable [1–3].

Coextensively with practical demonstrations of MFCs, advances in new technological solutions for every component of the fuel cell strive to improve its overall performance. The major engineering areas of interest consist of the anode, cathode [4–6], and microbial studies [7–9]. In addition, the separator between the electrodes is an important element, affecting the performance of MFCs as well as the other types of bioelectrochemical systems. One of the best studied materials used as

a membrane is Nafion, known for its good proton conductivity due to presence of sulphonate groups, a material used in MFCs for at least three decades [10]. In addition to ion exchange membranes [11] and modified Cation Exchange Membranes (CEM) such as Nafion-silica nanocomposites [12], several other types of membranes have been reported in the literature. Examples of such materials include natural materials, such as glass fibers, natural biodegradable materials such as natural rubber and ligno-cellulose, which has also found its application as sustainable material for gas diffusion layer [13–15]. Recent innovations have also demonstrated low-cost, high-efficiency materials such as ceramics to be a good substitute for conventional and costly cation exchange membranes (CEM) [16–19].

Another group of separators consists of synthetic materials such as nylon, polybenzimidazole, poly(vinyl alcohol) and ionic liquids, and various range of power densities and coulombic efficiencies have been reported [13,20–22]. Semi-synthetic materials such as starch and compostable polyester have also been successfully employed with a limited life-time due to their biodegradability [17].

The above-mentioned materials possess various important properties, however only one of them, Nafion, can be considered as a transparent material. The transparency may be a desirable quality for bioelectrochemical system and photobioreactor designs that require incident or transmitted light. Light transmission is desirable for the hybrid

* Corresponding author at: Laboratory for Artificial Biology, Centre for Integrative Biology, University of Trento, Polo Scientifico e Tecnologico Fabio Ferrari, Polo B, Via Sommarive 9, 38123 Povo TN, Italy.

E-mail address: grzegorz.pasternak@pwr.edu.pl (G. Pasternak).

photoreactor MFCs using algae or cyanobacteria as the biocatalysts or feedstock [23,24]. Nevertheless, the high cost of Nafion membranes remains as its main drawback.

In this paper we present the use of a natural silk fibroin membrane (SFM) as a CEM substitute. Silk fibroin is a protein produced by the silkworm. It has a compact beta-sheet structure, which makes this polymer slow to degrade over time. Silk fibroin can be isolated and regenerated to various forms such as powders, hydrogels, films and membranes [25,26]. Known for its biocompatibility [27], silk fibroin has been used in various applications apart from wound dressing such as enzyme immobilization [28], tissue engineering, and implants [29].

The SFM obtained by casting from different solvents can be tuned in terms of degradation and biocompatibility while retaining very high transparency. The biocompatibility of the silk fibroin would allow the use of this material in the emerging field of bioelectrochemistry such as implantable fuel cells and biosensors [30,31]. Although many interesting features of silk fibroin, only individual examples of their use in the field of electrochemistry are known. Xu et al. have fabricated reduced graphene oxide composites, using regenerated silk fibroin as a cost effective agent for the nanoparticles dispersion [32]. The obtained material was characterized by high catalytic activity for the oxygen reduction reaction. A study reported by Yun et al. showed, that silk fibroin can be also used to fabricate carbon-based nanoplates for the application in supercapacitors [33]. Nevertheless, to the best of our knowledge, the properties of silk fibroin have never been exploited in Microbial Fuel Cell based systems.

Here we assess the performance of SFM of varying fibroin density as a separator membrane in MFCs with regard to power performance, coulombic efficiency and longevity. The positive performance of the SFM signifies that a choice of synthetic and natural materials can be used to design and implement a completely transparent MFC. In the future, such transparent materials may be applied to induce the performance of bioelectrochemical photoreactors.

2. Materials and methods

2.1. Preparation of silk fibroin membranes (SFM)

Bombyx mori silkworm cocoons, kindly supplied by Chul Thai Silk (Petchaboon Province, Thailand) were degummed twice in 98 °C distilled water bath of Na₂CO₃ (Sigma, USA, 1.1 g/L and 0.4 g/L, respectively) for 1.5 h each. Then they were rinsed thoroughly with warm distilled (DI) water to remove the salt and completely dried at room temperature in a laminar flow hood. Degummed silk samples were dissolved in 9.3 M LiBr (Honeywell, Fluka, USA) water solution (2 g/10 mL) at 65 °C for 3 h, followed by dialysis against DI water with Slide-A-Lyzer Dialysis Cassettes (3500 MWCO, Pierce, USA) for 3 days to remove LiBr. Then the silk fibroin (SF) solution was filtered by 100–160 µm filter disc (DURAN, Mainz, Germany) to eliminate impurities. Purified SF solution was finally lyophilized (5Pascal, Milan, Italy) to obtain the SF powder.

SF powder was dissolved in formic acid (Honeywell, Fluka, USA) in different concentrations (2%, 4% and 8%, w/v) by stirring overnight at room temperature. The SF-formic acid solutions were cast into 100 mm cylindrical acrylic petri dishes and then dried overnight at room temperature in a laminar flow hood. The dried membranes were swelled in DI water for 3 h to make them flexible and then cut into round membranes (diameter of 55 mm) for use in MFCs or analysis. All the samples used in this study were prepared by using the same batch of SF powder and each concentration had three replicates.

2.2. MFC design and operation

The MFCs consisted of two chambers separated by either cation exchange membrane (CMI-7000, Membranes International, USA) or silk fibroin membrane (SFM) with three different concentrations: 2, 4 and 8%. Both anolyte and catholyte chambers were built from cylindrical

acrylic petri dishes (Sarstedt, Germany) with 55 mm diameter and 14 mm height. Each chamber contained circular feeding port (10 mm diameter) and was supplied with the electrode. Both cathode and anode electrodes were prepared by folding carbon veil (30 g/m², (PRF Composite Materials, Dorset, UK) into square shape giving a total surface area of 124 cm². The carbon veil was wrapped with the Nickel-chromium wire (Ø 0.45 mm, Scientific Wire Company, UK) in order to collect the electrons to the circuit. The membranes (both CEM and SFM) separating the chambers were assembled with the transparent petri dishes with the use of neutral silicone sealant (ITW Polymers, USA). Total surface area of the membranes was calculated to 23.7 cm². The calculated volume of the empty chamber was equal to 33.2 mL, while the measured displacement volume was estimated as 25.0 mL. All MFCs were prepared in triplicates. The MFC design is shown in Fig. 1A and B.

Anodic chambers of the MFCs were inoculated with the activated sludge derived from the aerobic chamber of municipal wastewater treatment plant (ADEP, Trento, IT). The inoculation was conducted during 2 days with 2 kΩ external load. After two days, the sludge was replaced with the mineral salt medium (MSM) supplemented with acetate as a single carbon source: 1.56 g/L KH₂PO₄, 2.67 g/L Na₂HPO₄·2H₂O, 0.50 g/L NH₄SO₄, 0.20 g/L MgSO₄·7H₂O, 0.01 g/L CaCl₂·2H₂O, 1 mL/L of a trace elements solution (Sigma Aldrich, Germany) and 0.1% sodium acetate. The cathode chamber was filled to its 75% with the tap water, leaving the remaining space empty to allow both sufficient hydration and oxygen exposure of the electrode. The above-mentioned procedure was repeated every 2 days as a batch feeding cycle.

2.3. Physical-chemical analysis and coulombic efficiency

Approximately every week, one day prior to polarisation experiments, the anolyte and catholyte were collected and pH was measured with a pH meter (Mettler Toledo, Switzerland). Samples collected after 2 weeks of operation have undergone the COD analysis. To remove the bacterial biomass, the samples were filtered with 0.2 µm syringe filter. The COD analysis was conducted using colorimetric COD test kit Spectroquant® (Merck Millipore, MA, US) according to the manufacturer's instructions.

The results from COD measurements and real time power performance monitoring were used to calculate the coulombic efficiency (CE) using the following equation (Logan et al., 2006):

$$CE = \frac{M \int_0^{t_b} Idt}{Fv_{an}\Delta COD} \quad (1)$$

Where: M - molecular weight of oxygen, F - Faraday's constant, b - the number of electrons exchanged per mole of oxygen, v_{An} - volume

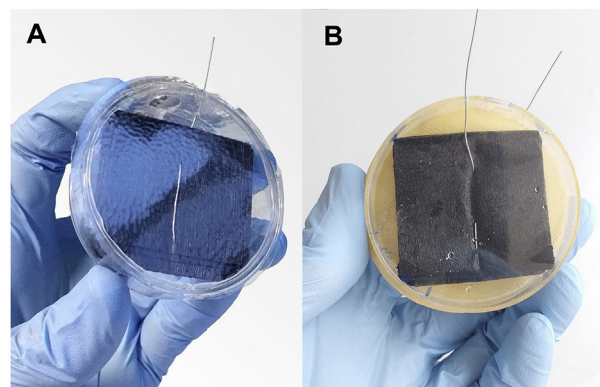


Fig. 1. Microbial Fuel Cell membrane appearance and Transmittance: A – transparent silk fibroin membranes (SFM), B – Cation exchange membranes (CEM).

of liquid in the anode compartment, ΔCOD - the change in COD over time t_b .

2.4. Flow cytometric analysis

Flow cytometric analysis was conducted on the samples after 15 and 29 days of operation. The aliquots of anolyte and catholyte samples were cryopreserved in 20% glycerol solution (v/v). In order to determine the number of bacterial cells in the catholyte and anolyte, the cryopreserved samples were thawed, centrifuged (12,000 RPM, 1 min), washed with filtered (0.2 μm) 0.85% NaCl solution and diluted to a concentration below 10^6 cells/mL. Afterwards, the samples were thermally fixed and stained using propidium iodide reaching its final concentration of 48 μM . Each sample was supplemented with approximately 100 counting beads (BD Biosciences, USA) and analysed using FACSCanto™ II system (BD Biosciences, USA). The samples were delivered to the interrogation point at a constant flow rate of 10 $\mu\text{L}/\text{min}$. Forward scatter (FSC), side scatter (SSC) and red fluorescence signal using 695/40 nm filter were recorded. The threshold was set up on FSC signal using filtered NaCl solution. The non-stained samples were used as control. Gating of the signal and enumeration of bacterial cells were conducted for combined SSC and red fluorescence (FL1) signal.

2.5. Polarisation experiments

Polarisation experiments were conducted approximately weekly. The experiments were conducted using decade boxes containing set of resistors to cover the resistance range of 102 Ω – 1 M Ω . Within this range, 20 individual resistors values were connected to the MFCs. Each resistance was connected to the MFC for a period of 5 min, after which the MFC potential was recorded and used for determining the polarisation curves.

2.6. Data logging and processing

The potential of each MFC was recorded using PicoLog ADC-24 Data Logger (Pico Technologies, UK) in real time, with the sampling rate set to 3 min. Current (in Amperes) and power (in Watts) were calculated according to Ohm's law:

$$I = V/R \quad (2)$$

$$P = I \cdot V \quad (3)$$

Where: V is the measured voltage in Volts (V), and R is the external resistance in Ohms (Ω).

The acquired data was processed using Microsoft Excel 2010 and visualised using GraphPad Prism software package.

2.7. Characterizations of silk fibroin membranes

All samples were characterized as cast (SFM_B) and after use in the MFCs (SFM_A) in order to assess the impact of the working conditions on membrane structure and stability.

2.8. Transparency

The transmittance measurements of samples as cast were conducted by using UV-Vis spectrophotometer (JASCO, VR-570, Japan) with wavelengths from 250 nm to 1000 nm. Three different points were selected and averaged for each sample.

2.9. Molecular weight

The molecular weight of SFMs_B and SFMs_A was determined by gel filtration chromatography (GFC). The GFC analysis was conducted with

Shodex SB-805 HQ column (Shodex OH pak®, 8.0 \times 300 mm, Showa Denko, Munich, Germany). The membranes were dissolved in 9.3 M LiBr water solution at 65 $^{\circ}\text{C}$ for 3 h, followed by dialysis against DI water with Slide-A-Lyzer Dialysis Cassettes (3500 MWCO, Pierce, USA) to remove LiBr. The obtained solutions were diluted with PBS solution (Sigma, USA) to reach a concentration in the range of 0.5–0.8 mg/mL. The chromatography was operated with a flow rate of 1 mL/min at 27 ± 1 $^{\circ}\text{C}$ and was detected with Jasco UV-1570 detector set (Jasco, Bouguenais, France) at 224 nm. The calibration curve was obtained with low/high molecular weight gel filtration calibration kit (GE Healthcare Europe, Freiburg, Germany).

2.10. Amino acid composition

The amino acid composition of silk fibroin powder and membranes was determined with the Waters AccQ-Fluor™ Reagent Kit using the AccQ-Tag™ amino acid analysis method (Waters Corp., Milford, MA, USA). For each sample, 4 mg was hydrolysed by 6 M HCl at 120 ± 2 $^{\circ}\text{C}$ in a silicone oil bath for 24 h. The air-dried hydrolysates were reconstituted with 20 mM HCl and then mixed with Waters AccQ-Fluor Reagent to obtain stable amino acids. The amino acid composition was determined by reverse phase high performance liquid chromatography (RP-HPLC) using an AccQ-Tag™ column (3.9 \times 150 mm, Waters Corp., Milford, MA, USA) with a gradient of Waters AccQ-Tag™ Eluent A, Milli-Q water, and Acetonitrile (HPLC grade). The amino acids were detected with the Jasco UV-1570 detector set (Jasco, Bouguenais, France) at 254 nm. The chromatograms obtained were compared with Waters Amino Acid Hydrolysate Standards.

2.11. Fourier transformation infrared spectroscopy

Fourier transform infrared spectroscopy (FTIR) analysis was performed on dried samples. Secondary structure analysis was determined by Fourier transform infrared spectroscopy (FTIR) in attenuated total reflectance (ATR) mode (FTIR-ATR, Spectrum One, PerkinElmer, USA) equipped with Zinc Selenide crystal on ATR. For each measurement, the spectrum collected in the range from 650 to 4000 cm^{-1} with 64 scans at the resolution of 4 cm^{-1} . Fourier self-deconvolution (FSD) of the infrared spectra covering Amide I region (1600–1700 cm^{-1}), peak finding and peak fitting were performed by Origin 2016 software.

In order to determine changes in the ratio of β -sheet compared with other secondary structures (α -helices, random coils and turns) induced by the working condition, the amide I band (1600–1700 cm^{-1}) was deconvoluted by using the method of Fourier self-deconvolution (FSD) (Hu et al, 2006). Peaks related to secondary structures were fitted inside the FSD amide I peak. The fitting was performed using Gaussian peak to calculate the percentage of content for each structure.

2.12. Thermal analysis

Thermal analysis was conducted by using a Differential Scanning Calorimeter (DSC, Q20, TA Instrument, USA), in nitrogen atmosphere with a heating rate of 10 $^{\circ}\text{C}/\text{min}$ using closed aluminum pans 3.00 mg–4.00 mg/sample, in the temperature range from 30 $^{\circ}\text{C}$ to 350 $^{\circ}\text{C}$. The degradation temperatures (T_d) and specific endothermic heat (ΔD) of each sample were determined.

2.13. Field emission scanning electron microscopy (FE-SEM)

SFMs_B were dried at room temperature in a laminar flow hood. The SFMs_A were first fixed in 4% glutaraldehyde in 0.1 M cacodylic buffer for 1 h at room temperature, followed by washing in 0.1 M cacodylate buffer (three times) and then dried at room temperature. All samples were sputter coated with Pt/Pd and then observed with Supra 40/40VP scanning electron microscope (SEM, Zeiss, Germany).

2.14. Water and ionic permeability

Two dedicated experiments were conducted to determine water and ionic permeability of SFM membranes. Water permeability was measured using 5 mL glass vials with internal diameter of 1.1 cm. Each vial was filled with deionized water, and SFMs in various concentrations along with CEM were fixed on the top tightly to avoid leaking. The bottles were incubated at 23 ± 1 °C and weighed every 24 h for a period of 8 days. Water vapour permeability was measured by calculating the weight lost in time.

The ionic permeability was measured using a dedicated dual-polypropylene chamber (internal diameter: 2.5 cm) with a membrane separating the chambers. Both chambers were filled with two PBS buffers (20 mL per chamber) at different pH: pH = 7.4 and pH = 9.0. The changes in pH were monitored by pH meter at constant temperature of 23 ± 1 °C every 24 h for a period of 8 days. All measurements were conducted in triplicates.

3. Results and discussion

3.1. MFC performance

MFCs were set up with three different SFM separators as well as an industry-standard CEM for performance comparison. The performance of the MFCs was assessed. Recording of the real time power performance revealed that 8% SFM reached almost as high performance (5.3 ± 3.8 μ W) as CEM (8.5 ± 0.8 μ W) after 5 days of operation. The performance of 4% and 2% SFMs was equal to 2.6 ± 1.1 μ W and 1.2 ± 0.8 μ W, respectively (Fig. 2A). The data derived from this initial period suggested that power performance of the MFCs could be positively correlated with the fibroin concentration in SFMs. This trend however has been reversed in the later stage, resulting in highest power performance of the SFM supplemented with the lowest (2%) concentration of the fibroin. The corresponding, maximal real time power performance over 30 days-period has been observed in the 24th day of operation and reached 25.7 ± 7.4 μ W, resulting in 68% of the performance of the

control CEM MFCs (37.7 ± 3.1 μ W). Performance recorded for 4% and 8% membranes was equal to: 15.2 ± 6.2 and 19.0 ± 0.8 μ W, respectively.

To further characterise the SFMs performance, polarisation experiments were conducted. After 15 days of operation, 2% SFM reached the highest power output of 12.8 ± 2.1 μ W, while 4 and 8% SFMs reached 8.6 ± 4.3 and 6.0 ± 4.9 μ W, correspondingly (Fig. 2C and D). Nevertheless, the performance of conventional CEM were twice as high and reached 26.7 ± 3.6 μ W. Similarly, the 2% SFM revealed the highest OCV of 315 ± 36 mV while 197 ± 100 and 144 ± 122 mV were observed for 4% and 8% SFMs, respectively and the CEM control reached 477 ± 13.4 mV. Therefore, the lowest fibroin concentration 2% SFMs outperformed the 4% and 8% SFMs, but their overall performance was lower than commercial, non-transparent CEM separators. The activation losses in all of the SFMs were less significant in comparison to CEM, which was a result of the lower OCV reached for all types of SFMs. The SFM-MFCs did not reveal significant ohmic losses, nor the power overshoot. As a result, the best-performing 2% SFM reached relatively high current output, comparable to the CEM control. The average current observed for 2% SFM was equal to 0.25 ± 0.03 mA, while for the CEM 0.29 ± 0.05 mA was observed. Therefore, the current reached by CEM control was only higher by 16% in comparison to the transparent SFM. Similarly as for power and voltage, the lowest current values were observed for 8% SFM.

Interestingly, all of the MFCs supplied with the SFM separators have reached lower R_{int} when compared to the CEM. After 15 days of operation the R_{int} observed for 2% SFMs was equal to 950 ± 320 Ω , while for 4% and 8% R_{int} values were lower and reached 900 ± 170 Ω and 500 ± 440 Ω , respectively. The R_{int} observed for CEM control was higher and reached 1080 ± 140 Ω . Along the whole experimental period, the internal resistance further decreased and stabilised between 430 and 530 Ω for 2% and 4% SFMs after 23 days of operation (Fig. 2B). Such low R_{int} values were not observed for the commercial CEM separators, which reached 630–830 Ω for a corresponding period. The recorded internal resistance was adversely proportional to the concentration of fibroin in SFM separators. Therefore, the low internal resistance of the MFCs supplied with SFM

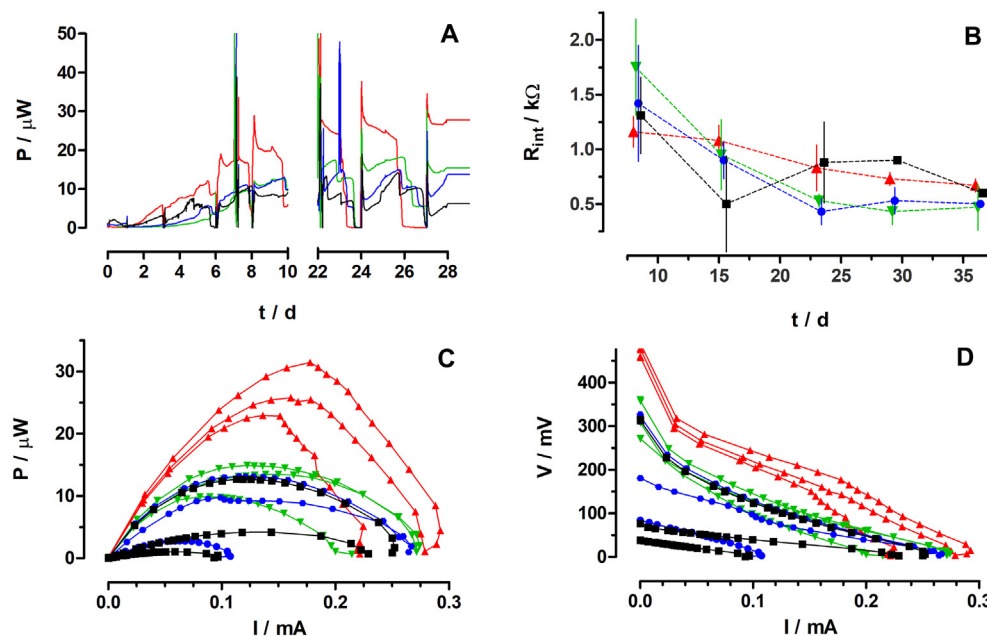


Fig. 2. Power performance of MFCs supplied with CEM (red lines, triangles), 2%-SFM (green lines, reversed triangles), 4%-SFM (blue lines, circles) and 8%-SFM (black lines, squares): A – Real time temporal performance of MFCs. Data represent average values from three replicates; B – The internal resistance change over time. Data with error bars represent average \pm SD. Data without error bars represent individual replicate, since the deteriorated (reversed) MFCs were excluded. For a better clarity, the datasets were shifted for a factor of 0.2 on time-axis; C and D – Polarisation and power curves obtained after 15 days of operation. Data represent individual replicates.

separators was caused by the low resistance of SFM separators rather than conductive biofilm properties at the anodes.

Low membrane resistance was commonly reported for different types of porous membranes. Several studies reported that synthetic porous membranes possess lower internal resistance which initially leads to increased power performance that later deteriorates due to the oxygen and substrates cross-over [11]. Pasternak et al. described that porosity also plays a crucial role in establishing low R_{int} and high power efficiency of different types of ceramic separators [18]. Although the SFM membranes are not porous, they may encounter similar problems as the porous materials due to their high oxygen diffusion coefficients when compared to Nafion material [34,35]. It is noteworthy, that SFM separators used in this study had approximately 10 times lower thickness than the CEM. The thickness of the SFM separators tested (52–58 μm) is one of the lowest values reported for MFCs, which typically range between 190 and 460 μm for polymeric membranes [36]. Such a low thickness could contribute to the oxygen and substrate cross-over. Internal resistance (R_{int}) values may be affected by several factors such as dynamics of the biofilm development [37] or membrane properties. In present study low thicknesses explains the low R_{int} values that were observed throughout the experimental period. In further research, this parameter will require optimisation, to remove the undesirable effects that may suppress the overall MFC performance.

3.2. COD and pH changes

The highest COD removal was observed for the 4% SFM. The COD decreased to $60.7 \pm 10.1 \text{ mgO}_2/\text{L}$, which corresponded to $93.9 \pm 1.0\%$ COD removal. Similar COD removal efficiency was observed for 8% SFM (Fig. 3A and B). Nevertheless observed coulombic efficiencies were similar and equal to 4.88%. The highest COD (lowest COD removal) values were observed for 2% SFM and CEM separators reaching $158.3 \pm 70.1 \text{ mgO}_2/\text{L}$ ($84.2 \pm 7.0\%$ removal) $315.7 \pm 183.9 \text{ mgO}_2/\text{L}$ ($68.4 \pm 18.4\%$ removal) for 2% SFM and CEM, correspondingly. In contrast to the COD removal efficiency, the 2% SFM and CEM separators have reached

the highest CE levels of $6.65 \pm 1.90\%$ (2% SFM) and $8.96 \pm 2.89\%$ (CEM). Therefore, MFCs supplied with 2% SFM separators have reached 74% of coulombic efficiency observed for the commercial, non-transparent CEM. The highest COD removal was observed for 2% and 4% SFM along with the lowest coulombic efficiencies. Therefore, the majority of the substrate was consumed throughout the fermentation or other metabolic pathways such as aerobic respiration due to potential microaerophilic conditions. The CE values are dependent on several factors among which MFC design, composition and metabolism of the electroactive community are the main ones. In this study, simple design with carbon veil as the cathode and anode electrode was used. Thus observed values both for the control and SFM were lower when compared to the other studies concerning polymer separators [38].

The pH of the catholyte rose throughout the experimental period in all of the MFC types. At the end of experimental period (28 days) the pH of the catholyte with SFM separators reached between 7.84 and 8.24. While for CEM, the observed pH was 9.47. We observe that the CEM catholyte reached the highest pH values as well as the greatest disproportion in pH between anodic and cathodic chambers in comparison with SFM separators. This phenomenon is commonly caused by ionic imbalance and may have a deteriorating effect on the MFC power performance [39]. Moreover, the pH values for SFM separators revealed positive correlation with fibroin concentration, while values observed for CEM MFCs showed a negative correlation (correlation coefficients were further evaluated in supporting information). Both low difference and correlation observed for pH values in SFM MFC chambers were in line with the lower performance. We believe that deterioration of the membranes caused the diffusion of the electrolyte between the chambers and resulted in lower pH difference, as well as lower overall MFCs performance. The physical and biological degradation of the membranes (discussed in Section 3.4) could have acted concomitantly with the lack of permselectivity of the membranes for protons. Although 4% and 8%-SFM revealed similar water transport properties to CEM (Fig. S1A), the permeability of SFM for Na^+ and OH^- ions was much higher when compared to CEM (Fig. S1B). This lack of selectivity as

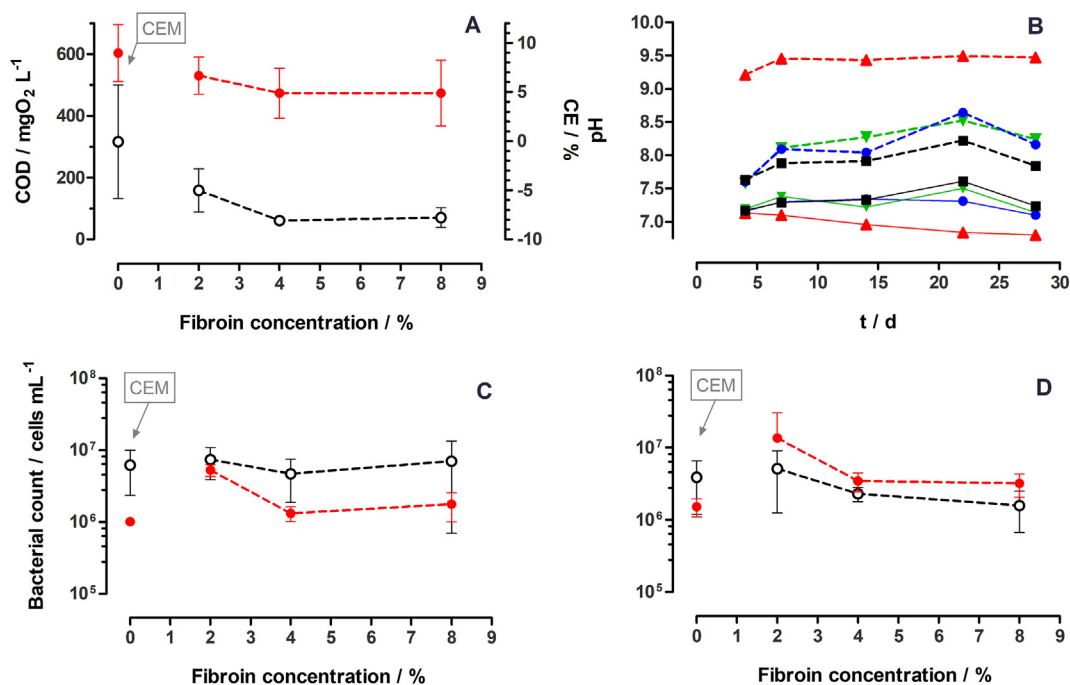


Fig. 3. Physical, chemical and biological characterisation of MFCs: A – COD (empty circles) and coulombic efficiency (filled circles) determined 3 days after feeding in batch conditions and after 15 days of operation, B – pH changes over time in anodic (solid lines) and cathodic (dashed lines) chambers for CEM (red triangles), 2%-SFM (green reversed triangles), 4%-SFM (blue circles), 8% (black squares). Data indicated for 0% corresponds to the CEM control. C and D – Total bacterial count in anodic (empty circles) and cathodic (filled circles) chambers determined by flow cytometry after 15 (C) and 29 days (D) of operation. Data indicated for 0% corresponds to CEM control. The values represent average from three replicates \pm SD.

well as material deterioration were reflected by the smaller difference in pH between the anode and cathode compartments in SFM MFCs when compared to CEM MFCs.

3.3. Characterizations of silk fibroin membranes

SFMs were produced by using different protein concentrations and formic acid as solvent. Physical and chemical properties of SFMs before (SFMs_B) and after use in the MFCs (SFMs_A) were investigated by using multiple methods in order to evaluate the impact of the complex working environment. Considering this, three main physical factors may be apparent: protein degradation, conformational changes and intermolecular and intramolecular bonding. In our work, structures and performances of SFMs were evaluated in a working environment with contributions from all potential aging mechanisms.

The transparency of the SFMs was assessed (Fig. S2) and all samples showed plateau with transmittance around 90% over the visible range (400–700 nm). Samples 2% and 8% showed a little decrease in transparency that became more evident in sample 4%. After use the transparency was affected by the biofilm deposition (Fig. 4). However, despite the biofilm presence the transparency values obtained after use, in particular on samples 2% and 8%, were close to the initial values. High transparency reveals great advantage of using SFM in novel, photobioelectrochemical reactors.

The amino acid composition (mol %) of fibroin heavy chain before use (Table S1) was composed by glycine (Gly, 49.1%), alanine (Ala, 31.1%) and serine (Ser, 5.7%) that forms the crystalline regions (hexapeptide) of the molecule together with Tyrosine (Tyr, 4.7%) and Valine (Val, 2.6%), while the amorphous regions were highly enriched in amino acids with bulky and polar side chains. Amino acid composition of SFMs after use (SFMs_A) was compared with the silk fibroin powder (Table S1), in order to evaluate possible degradation of the material. The degradation impact was seen to affect mainly the hexapeptide blocks but in a various ways depending on the concentration of original SF solution. When considering the amino acids involved in the hexapeptide composition (Gly, Ala, Ser, Tyr and Val), samples after use showed a decrease in concentration of 2.1%, 3.3% and 3.6% for 2%, 4% and 8% SFMs respectively. Such a decrease is not in agreement with the enzymatic degradation as reported by Arai et al [40], thus suggesting the possible role of electric field on such changes. We note that such compositional effects would be affected by the presence of a biofilm on the membrane. The overall degradation of SFMs was attributable to cleavage of the fibroin chains and release of a range of soluble peptides, thus changing the amino acid composition and molecular weight of the protein.

Fibroin molecular weight (Mw) data (Table S3) showed that 2% (from 223.165 kDa, PDI: 4.99 to 277.459 kDa, PDI: 6.11) and 4% SFMs (from 255.410 kDa, PDI: 5.13 to 270.773 kDa, PDI: 6.95) had an increase of the average size of protein molecule after use, while for 8%, a decrease of molecular weight was observed (from 318.563 kDa, PDI: 5.36 to 295.470 kDa, PDI: 6.69). It should be stated that these data could be affected by the presence of bacteria and biofilm (Fig. 4). DSC curves of all the samples were reported in Fig. 5A. All samples showed the first wide endothermic peak with similar associated areas indicating water evaporation. In particular, for 2% and 4% SFMs before and after use, this peak was centred around 80 °C to 84 °C whereas for 8% SFMs the centre of the peak before and after use was 92.9 °C (134.3 J g⁻¹) and 83.1 °C (195.5 J g⁻¹), respectively. Crystallization peak at around 212 °C [41] was not detected in all samples confirming that β -sheet formation occurred due to the evaporation of formic acid [42] during the preparation process. 2% and 4% SFMs showed the similar results. Focussing on 2% SFMs, the degradation peak before and after use had a slight increase from 277.3 °C (131.2 J g⁻¹) to 279.4 °C (174.1 J g⁻¹) suggesting degradation of insoluble helices [41], and with a shoulder centred at 282.5 °C which was related to the degradation of more stable β -sheet structure [43]. On the contrary, 8% SFMs had a decrease of the degradation peak,

from 281.3 °C (111.6 J g⁻¹) to 277.6 °C (163.9 J g⁻¹) after use with a shoulder shifting from 277.1 °C to 281.8 °C. To better understand the samples' thermal behaviour, the FTIR analysis was performed to evaluate the protein conformational changes.

All samples' FTIR curves clearly showed the presence of β -sheet secondary conformation (Fig. 5B). The amide I and amide II peaks for all SFMs before and after use showed a strong and sharp peak at 1621 and 1515 cm⁻¹ respectively, which were typical regions for β -sheet conformation. Antiparallel type β form was detected at 1696 cm⁻¹. Weak shoulders at 1648 cm⁻¹ suggested the progressively shifting from random coil to β -sheet structure during formic acid evaporation. The presence of β -sheet conformation was confirmed by the Amide III peak centred at 1230 cm⁻¹ with a shoulder at 1264 cm⁻¹ [41].

Considering secondary structure analysis of samples before use, 8% SFM displayed a higher content of β -sheet (62.2%) and lower content of random coil (11.2%), α -helices (12.6%) and turns (13.9%), in comparison with 2% and 4% SFM (Fig. 5C). The lower volatility of formic acid in 8% formulation induced a local ordering of chains, so increasing the amount of β -sheet [42]. Referring to Bucciarelli et al [42], samples' crystallites should be very small because they do not interfere with the optical properties as underlined by the transmittance measurements on cast membranes (Fig. 1C). After use, depending on the formulation (fibroin percentage), the working environment had different impacts on secondary conformation of fibroin as well as on intermolecular and intramolecular β -sheet structure (Fig. 5D). In 2% SFM, most of the random coils transformed into α -helices, maintaining the ratio between intermolecular and intramolecular β -sheet stable. In 4% and 8%, it was observed the similar trend, increasing of turns, α -helices and decreasing of β -sheet but much more evident in the higher protein concentration (Fig. 5C). Moreover the intermolecular β -sheet in 8% SFM_A dropped to 24% (47% compared with 8% SFM_B), while intramolecular interaction increased up to 22.1%. These changes in protein structure were in good agreement with the observed decrease of degradation temperature in DSC curve (from 281.3 °C to 277.6 °C), indicating that material instability increased during experiment and also explaining the observed leakage of membrane. This type of protein behaviour was already described when fibroin membranes were cast in electric field. This suggests that the electric field generated across the SFM could be a primary factor in the physical changes observed here. As reported previously, the electric field can affect fibroin folding, in particular β -sheet intermolecular bonds [44].

Water permeability of 2% SFM was different from 4 and 8% membranes. By changing the concentration of fibroin, different protein assemblies and secondary structures can be induced which changes the association of the protein matrix with water [35,45]. This change in structure and association with water can be partially tuned by changing the percentage of fibroin. In addition water permeability is expected to eventually plateau with higher fibroin content, as observed in Fig. S2A.

3.4. Biofouling and deterioration of the membranes

Flow cytometric measurements of total (living and dead) bacterial populations showed that after 15 days of operation the anodic communities in both SFM and control CEM MFCs were of a similar size and ranged between $4.67 \times 10^6 \pm 2.79 \times 10^6$ and $7.40 \times 10^6 \pm 3.51 \times 10^6$ cells/mL (Fig. 3C). Lower cell densities were observed in cathodic chambers, both in control CEM and SFM-supplied MFCs. The lowest population size was observed for the control MFCs and reached $1.01 \times 10^6 \pm 9.07 \times 10^4$ cells/mL. After 29 days of operation, the cathodic environment was more abundant in bacterial cells for all of the SFM membranes (Fig. 3D). The observed cell densities in the catholyte exceeded those observed for the anolyte. Such a change was not observed for the CEM membranes. Therefore, the cathodic environment established in CEM MFCs was suppressing the growth of bacterial community. Exceeding 15 days of SFM operation resulted in higher bacterial numbers recorded in cathodic chamber in comparison to anodic chamber. When

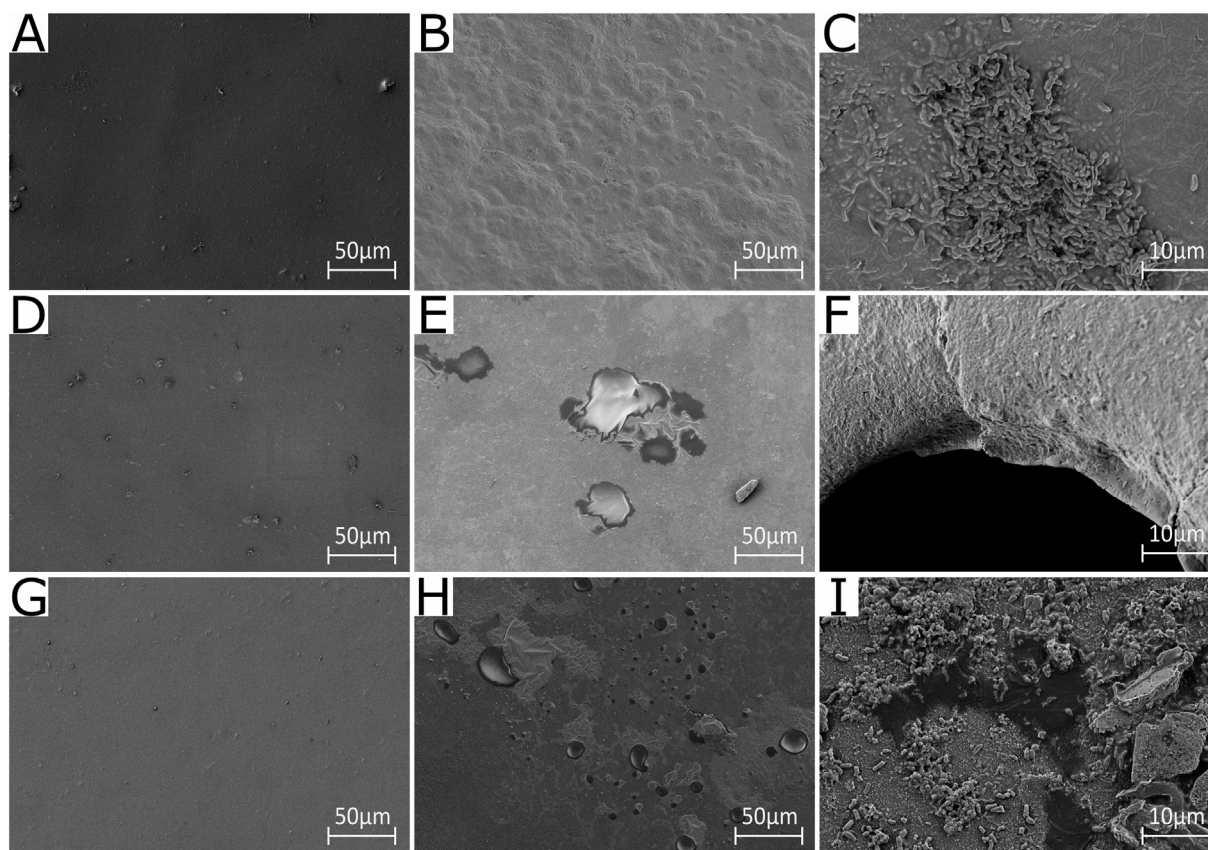


Fig. 4. FE-SEM images of SFMs in different concentration before and after use. A, D and G were SFMs before use in 2%, 4% and 8% (magnification 1000), respectively, B, E and H were SFMs after use in 2%, 4% and 8% (magnification 1000), respectively, C, F and I were SFMs after use in 2%, 4% and 8% (magnification 5000), respectively.

comparing the CEM control, the results suggest that physical and biological deterioration of SFM separators could have affected the cathodic community and induce its growth. In particular relatively low pH observed in SFM cathodic chamber along with abundance of oxygen and substrate cross-over could have resulted in development of aerobic microflora which negatively affected the overall MFC performance. Undesirable aerobic growth of bacteria in the cathode compartment may result in competition for the oxygen and affect its availability for the oxygen reduction reaction [46–48]. Lower cell densities observed in catholyte of CEM control were a result of high alkaline conditions, which is a result of an ionic imbalance [39].

The FE-SEM analysis conducted on SFM separators at the end of experiment revealed, that each type of the separator have undergone the biofouling process (Fig. 4). At the surface of the membranes several microstructural changes of various morphology have been also observed. Such phenomena are commonly reported at the interface of the separator and electrodes as a result of biofouling and salt precipitation [18,49–52]. The biofilm covering the membranes was rich in EPS which suggests, that its metabolism rate was rather low [53]. More spots with the exposed cells were detected at the 8% SFM surface. The biofilm could have been the major factor inducing deterioration of the membranes, which can be seen for each type of the SFM separator. However, the morphology of deteriorated microstructure varied across different concentrations of fibroin. Phenomena such as enhanced cracking due to precipitate deposits were observed in particular for 8%, but also for 4% SFMs, while larger biofilm-free and membrane-loss areas were mainly observed for 4% and 2% SFMs. All the above mentioned microstructural changes are typical for the biodegradation process initiated by microorganisms [54,55]. This microstructural changes observed

by FE-SEM, were in well agreement with FTIR data, in particular with the decreasing of β -sheet intermolecular bonding observed in 8% SFM. We believe, that those morphological and structural changes indicated the biodegradability of the silk fibroin membranes (physical crosslinked) in the MFC environment and could be the main reason for enhanced nutrient and oxygen crossover. Such a feature however, may be beneficial for several types of the MFC applications such as biodegradable fuel cells, which are intended to operate in the environment for a specific period of time and leave minimal environmental impact afterwards.

3.5. Deterioration of the power output

In the first two weeks all of the MFCs were operational, i.e. producing power. After 24 days however, one of the 8% replicate MFCs failed and its performance was never recovered. Similarly, cell reversal was observed later on: after 28 days only one of the 8% replicates was not reversed. After 32 days, also one of the 4% replicates has reversed and only 2% SFM triplicates remained stable. Therefore, decreasing performance was first noticed for the SFMs with the higher concentration of fibroin suggesting that it was the fibroin component which was controlling the deterioration of the membranes. Silk fibroin membranes are known for their biodegradability and the observed biodegradation periods varies from weeks to months [56]. Since the SFM power deterioration was dependent on fibroin concentration, we believe that physical and biological deterioration of the membranes could have been responsible for the observed drop in performance.

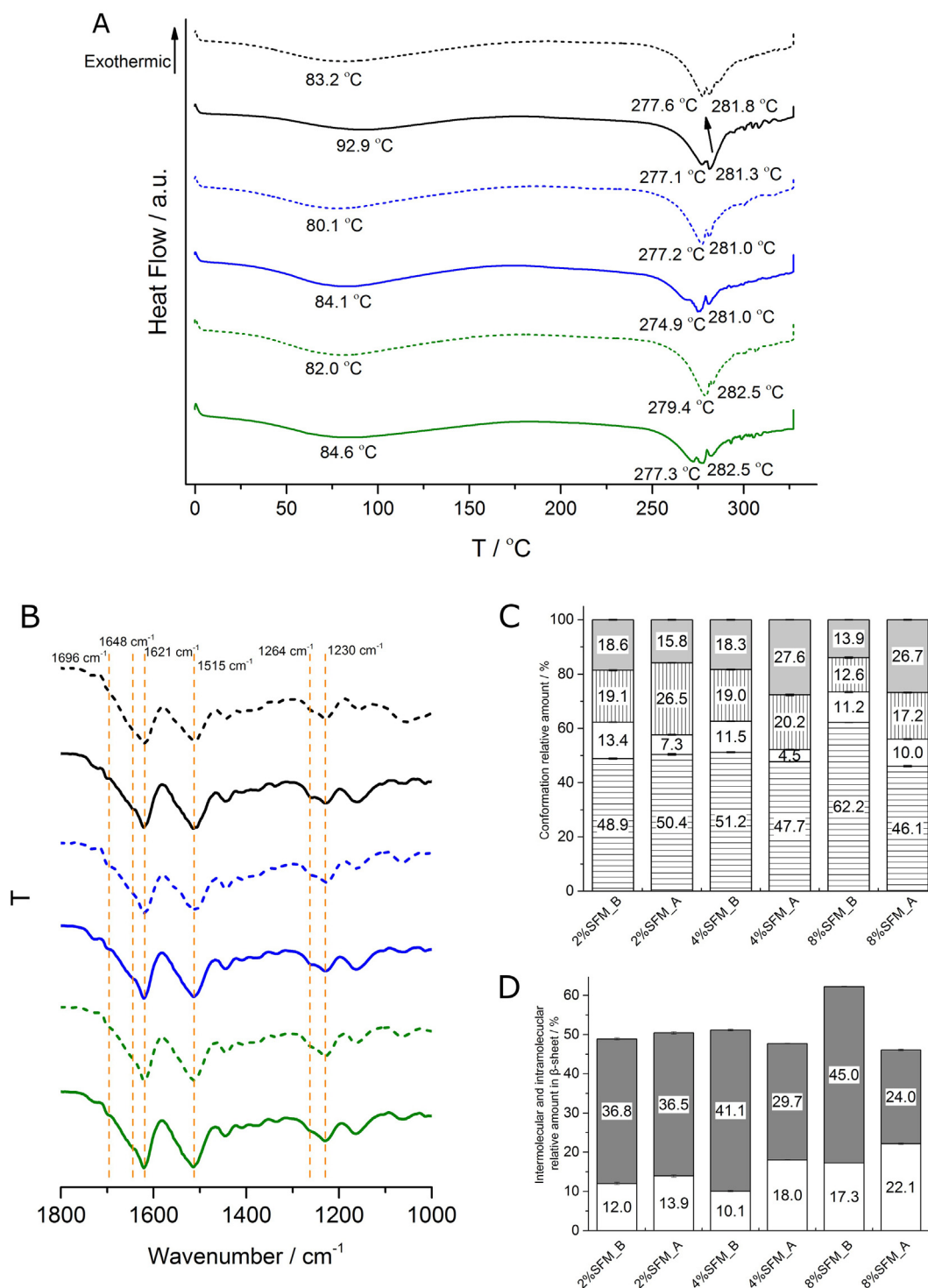


Fig. 5. Chemical characterizations of SFMs in different concentration before and after use: A – DSC curves and B – FTIR spectra of SFMs before (solid lines) and after (dash lines) use in different concentrations (2%-SFM – green, 4%-SFM – blue and 8%-SFM – black). C – Relative contributions of β-sheet (horizontal lines), random coil (white), α-helix (vertical lines) and turns to amide I area in SFMs before and after use. D – The ratio of intermolecular (grey) and intramolecular (white) bonding of β-sheet.

4. Conclusions

We have introduced transparent fibroin membranes in MFCs and determined the influence of fibroin concentration on MFC performance. The performance of SFM was dependent on SFM concentration and the best results were achieved for the 2%-SFM. Deterioration of the membranes and their performance observed after one month of operation was stronger for the high fibroin-

content SFMs (4% and 8%). The transparent quality of the SFM separators was not significantly altered over the course of the MFC operation despite of biofouling. The properties of SFMs make them an appropriate material for novel applications of bioelectrochemical systems, where the light transmission, biodegradability and biocompatibility are required.

Supplementary data to this article can be found online at <https://doi.org/10.1016/j.bioelechem.2018.12.004>.

Acknowledgements

This work has been partially funded by the European Union's Horizon 2020 research and innovation programme under the grant 686585 - LIAR, Living Architecture.

References

- [1] S. Choi, J. Chae, Sensors and actuators a : physical an array of microliter-sized microbial fuel cells generating 100 W of power, *Sensors Actuators A Phys.* 177 (2012) 10–15, <https://doi.org/10.1016/j.sna.2011.07.020>.
- [2] I.A. Ieropoulos, A. Stinchcombe, I. Gajda, S. Forbes, I. Merino-Jimenez, G. Pasternak, D. Sanchez-Herranz, J. Greenman, Pee power urinal – microbial fuel cell technology field trials in the context of sanitation, *Environ. Sci. Water Res. Technol.* 2 (2016) 336–343, <https://doi.org/10.1039/C5EW00270B>.
- [3] Z. Ge, L. Wu, F. Zhang, Z. He, Energy extraction from a large-scale microbial fuel cell system treating municipal wastewater, *J. Power Sources* 297 (2015) 260–264, <https://doi.org/10.1016/j.jpowsour.2015.07.105>.
- [4] X. Zhang, W. He, R. Zhang, Q. Wang, P. Liang, High-Performance Carbon Aerogel Air Cathodes for Microbial Fuel Cells, 2016 2788–2795, <https://doi.org/10.1002/cssc.201600590>.
- [5] C. Santoro, R. Gokhale, B. Mecheri, A.D. Epifanio, Design of Iron (II) Phthalocyanine-Derived Oxygen Reduction Electrocatalysts for High-Power-Density Microbial Fuel Cells, 2017 3243–3251, <https://doi.org/10.1002/cssc.201700851>.
- [6] M. Grattieri, N.D. Shivel, I. Sifat, M. Bestetti, S.D. Minter, Sustainable hypersaline microbial fuel cells: inexpensive recyclable polymer supports for carbon nanotube conductive paint anodes, *ChemSusChem* 10 (2017) 2053–2058, <https://doi.org/10.1002/cssc.201700099>.
- [7] E.S. Heidrich, J. Dolfing, M.J. Wade, W.T. Sloan, C. Quince, T.P. Curtis, Temperature, inocula and substrate: contrasting electroactive consortia, diversity and performance in microbial fuel cells, *Bioelectrochemistry* 119 (2018) 43–50, <https://doi.org/10.1016/j.bioelechem.2017.07.006>.
- [8] L. Rago, S. Zecchin, S. Marzorati, A. Goglio, L. Cavalca, P. Cristiani, A. Schievano, A study of microbial communities on terracotta separator and on biocathode of air breathing microbial fuel cells, *Bioelectrochemistry* 120 (2018) 18–26, <https://doi.org/10.1016/j.bioelechem.2017.11.005>.
- [9] I. Ieropoulos, G. Pasternak, J. Greenman, Urine disinfection and in situ pathogen killing using a microbial fuel cell cascade system, *PLoS ONE* 12 (2017) <https://doi.org/10.1371/journal.pone.0176475>.
- [10] H.P. Bennetto, J.L. Stirling, K. Tanaka, C. a Vega, Anodic reactions in microbial fuel cells, *Biotechnol. Bioeng.* 25 (1983) 559–568, <https://doi.org/10.1002/bit.260250219>.
- [11] J.X. Leong, W.R.W. Daud, M. Ghasemi, K. Ben Liew, M. Ismail, Ion exchange membranes as separators in microbial fuel cells for bioenergy conversion: a comprehensive review, *Renew. Sust. Energ. Rev.* 28 (2013) 575–587, <https://doi.org/10.1016/j.rser.2013.08.052>.
- [12] S. Angioni, L. Millia, G. Bruni, C. Tealdi, P. Mustarelli, E. Quartarone, Improving the performances of Na fi on TM-based membranes for microbial fuel cells with silica-based , organically-functionalized mesostructured fi llers, *J. Power Sources* 334 (2016) 120–127, <https://doi.org/10.1016/j.jpowsour.2016.10.014>.
- [13] X. Zhang, S. Cheng, X. Huang, B.E. Logan, The use of nylon and glass fiber filter separators with different pore sizes in air-cathode single-chamber microbial fuel cells, *Energy Environ. Sci.* 3 (2010) 659, <https://doi.org/10.1039/b927151a>.
- [14] J. Winfield, I. Ieropoulos, J. Rossiter, J. Greenman, D. Patton, Biodegradation and proton exchange using natural rubber in microbial fuel cells, *Biodegradation* 24 (2013) 733–739, <https://doi.org/10.1007/s10532-013-9621-x>.
- [15] S. Marzorati, A. Schievano, A. Colombo, G. Lucchini, Ligno-cellulosic materials as air-water separators in low-tech microbial fuel cells for nutrients recovery, *J. Clean. Prod.* 170 (2018) 1167–1176, <https://doi.org/10.1016/j.jclepro.2017.09.142>.
- [16] M. Behera, P.S. Jana, M.M. Gharekhar, Performance evaluation of low cost microbial fuel cell fabricated using earthen pot with biotic and abiotic cathode, *Bioresour. Technol.* 101 (2010) 1183–1189, <https://doi.org/10.1016/j.biortech.2009.07.089>.
- [17] J. Winfield, L.D. Chambers, J. Rossiter, I. Ieropoulos, Comparing the short and long term stability of biodegradable, ceramic and cation exchange membranes in microbial fuel cells, *Bioresour. Technol.* 148 (2013) 480–486, <https://doi.org/10.1016/j.biortech.2013.08.163>.
- [18] G. Pasternak, J. Greenman, I. Ieropoulos, Comprehensive study on ceramic membranes for low-cost microbial fuel cells, *ChemSusChem* 9 (2016) 88–96, <https://doi.org/10.1002/cssc.201501320>.
- [19] A. Tremouli, J. Greenman, I. Ieropoulos, Investigation of ceramic MFC stacks for urine energy extraction, *Bioelectrochemistry* 123 (2018) 19–25, <https://doi.org/10.1016/j.bioelechem.2018.03.010>.
- [20] S. Angioni, L. Millia, G. Bruni, D. Ravelli, P. Mustarelli, E. Quartarone, Novel composite polybenzimidazole-based proton exchange membranes as efficient and sustainable separators for microbial fuel cells, *J. Power Sources* 348 (2017) 57–65, <https://doi.org/10.1016/j.jpowsour.2017.02.084>.
- [21] G. Chen, F. Zhang, B.E. Logan, M.a. Hickner, Poly(vinyl alcohol) separators improve the coulombic efficiency of activated carbon cathodes in microbial fuel cells, *Electrochem. Commun.* 34 (2013) 150–152, <https://doi.org/10.1016/j.elecom.2013.05.026>.
- [22] A.M. Rubio, A. Gim, A.P.D.L.R. M.J. Salar-Garc, V.M. Ortiz-Mart, F.J. Hern, Influence of Ionic Liquid Composition on the Stability of Polyvinyl Chloride-Based Ionic Liquid Inclusion Membranes in Aqueous Solution, 00, 2016 1–11, <https://doi.org/10.1002/aic>.
- [23] M. Rosenbaum, U. Schröder, F. Scholz, Utilizing the green alga *Chlamydomonas reinhardtii* for microbial electricity generation: a living solar cell, *Appl. Microbiol. Biotechnol.* 68 (2005) 753–756, <https://doi.org/10.1007/s00253-005-1915-4>.
- [24] S.B. Velasquez-Orta, T.P. Curtis, B.E. Logan, Energy from algae using microbial fuel cells, *Biotechnol. Bioeng.* 103 (2009) 1068–1076, <https://doi.org/10.1002/bit.22346>.
- [25] N. Minoura, S.I. Aiba, M. Higuchi, Y. Gotoh, M. Tsukada, Y. Imai, Attachment and growth of fibroblast cells on silk fibroin, *Biochem. Biophys. Res. Commun.* 208 (1995) 511–516, <https://doi.org/10.1006/bbrc.1995.1368>.
- [26] C. Acharya, S.K. Ghosh, S.C. Kundu, Silk fibroin protein from mulberry and non-mulberry silkworms: cytotoxicity, biocompatibility and kinetics of L929 murine fibroblast adhesion, *J. Mater. Sci. Mater. Med.* 19 (2008) 2827–2836, <https://doi.org/10.1007/s10856-008-3408-3>.
- [27] M. Santin, A. Motta, G. Freddi, M. Cannas, In vitro evaluation of the inflammatory potential of the silk fibroin, *J. Biomed. Mater. Res.* 46 (1999) 382–389, [https://doi.org/10.1002/\(SICI\)1097-4636\(19990905\)46:3<382::AID-JBM11>3.0.CO;2-R](https://doi.org/10.1002/(SICI)1097-4636(19990905)46:3<382::AID-JBM11>3.0.CO;2-R).
- [28] S. Yi, F. Dai, Y. Ma, T. Yan, Y. Si, G. Sun, Ultrafine silk-derived nanofibrous membranes exhibiting effective lysozyme adsorption, *ACS Sustain. Chem. Eng.* 5 (2017) 8777–8784, <https://doi.org/10.1021/acssuschemeng.7b01580>.
- [29] L. Meinel, R. Fajardo, S. Hofmann, R. Langer, J. Chen, B. Snyder, G. Vunjak-Novakovic, D. Kaplan, Silk implants for the healing of critical size bone defects, *Bone* 37 (2005) 688–698, <https://doi.org/10.1016/j.bone.2005.06.010>.
- [30] M. Frei, J. Erben, J. Martin, R. Zengerle, S. Kerzenmacher, Nano fiber-deposited porous platinum enables glucose fuel cell anodes with high current density in body fluids, *J. Power Sources* 362 (2017) 168–173, <https://doi.org/10.1016/j.jpowsour.2017.07.001>.
- [31] A. PrévotEAU, K. Rabaey, Electroactive biofilms for sensing: reflections and perspectives, *ACS Sensors* 2 (2017) 1072–1085, <https://doi.org/10.1021/acssensors.7b00418>.
- [32] S. Xu, L. Yong, P. Wu, One-Pot, Green, Rapid Synthesis of Flowerlike Gold Nanoparticles/Reduced Graphene Oxide Composite with Regenerated Silk Fibroin As Efficient Oxygen Reduction Electrocatalysts, 2013.
- [33] Y.S. Yun, S.Y. Cho, J. Shim, B.H. Kim, S. Chang, S.J. Baek, Y.S. Huh, Y. Tak, Y.W. Park, S. Park, Microporous Carbon Nanoplates from Regenerated Silk Proteins for Supercapacitors, 2013 1993–1998, <https://doi.org/10.1002/adma.201204692>.
- [34] K. Kudo, R. Jinnouchi, Y. Morimoto, Humidity and temperature dependences of oxygen transport resistance of nafion thin film on platinum electrode, *Electrochim. Acta* 209 (2016) 682–690, <https://doi.org/10.1016/j.electacta.2016.04.023>.
- [35] B. Marelli, M.A. Brenckle, D.L. Kaplan, F.G. Omenetto, Silk fibroin as edible coating for perishable food preservation, *Sci. Rep.* 6 (2016), 25263, <https://doi.org/10.1038/srep25263>.
- [36] W.-W. Li, G.-P. Sheng, X.-W. Liu, H.-Q. Yu, Recent advances in the separators for microbial fuel cells, *Bioresour. Technol.* 102 (2011) 244–252, <https://doi.org/10.1016/j.biortech.2010.03.090>.
- [37] G. Pasternak, J. Greenman, I. Ieropoulos, Dynamic evolution of anodic biofilm when maturing under different external resistive loads in microbial fuel cells. Electrochemical perspective, *J. Power Sources* 400 (2018) 392–401, <https://doi.org/10.1016/j.jpowsour.2018.08.031>.
- [38] G. Chen, B. Wei, Y. Luo, B.E. Logan, M.A. Hickner, Polymer separators for high-power, high-efficiency microbial fuel cells, *ACS Appl. Mater. Interfaces* 4 (2012) 6454–6457, <https://doi.org/10.1021/am302301t>.
- [39] R.A. Rozendal, H.V. Hamelers, C.J. Buisman, Effects of membrane cation transport on pH and microbial fuel cell performance, *Environ. Sci. Technol.* 40 (2006) 5206–5211 <http://www.ncbi.nlm.nih.gov/pubmed/16999090>.
- [40] T. Arai, G. Freddi, R. Innocenti, M. Tsukada, Biodegradation of bombyx mori silk fibroin fibers and films, *J. Appl. Polym. Sci.* 91 (2004) 2383–2390, <https://doi.org/10.1002/app.13393>.
- [41] E. Callone, S. Dirè, X. Hu, A. Motta, Processing influence on molecular assembling and structural conformations in silk fibroin: elucidation by Solid-state NMR, *ACS Biomater. Sci. Eng.* 2 (2016) 758–767, <https://doi.org/10.1021/acsbiomaterials.5b00507>.
- [42] A. Bucciarelli, R.K. Pal, D. Maniglio, A. Quaranta, V. Mulloni, A. Motta, V.K. Yadavalli, Fabrication of nanoscale patternable films of silk fibroin using benign solvents, *Macromol. Mater. Eng.* 302 (2017) 1–9, <https://doi.org/10.1002/mame.201700110>.
- [43] Q. Lu, B. Zhang, M. Li, B. Zuo, D.L. Kaplan, Y. Huang, H. Zhu, Degradation mechanism and control of silk fibroin, *Biomacromolecules* 12 (2011) 1080–1086, <https://doi.org/10.1021/bm101422j>.
- [44] E. Servoli, D. Maniglio, A. Motta, C. Migliaresi, Folding and assembly of fibroin driven by an AC electric field: effects on film properties, *Macromol. Biosci.* 8 (2008) 827–835, <https://doi.org/10.1002/mabi.200800057>.
- [45] C. To, E. Preparation, Physico-chemical properties of silk fibroin membrane as a biomaterial, *Biomaterials* 11 (1990) 430–434.
- [46] M. Oliot, L. Etcheverry, A. Bergel, Removable air-cathode to overcome cathode biofouling in microbial fuel cells, *Bioresour. Technol.* 221 (2016) 691–696, <https://doi.org/10.1016/j.biortech.2016.09.095>.
- [47] G. Pasternak, J. Greenman, I. Ieropoulos, Regeneration of the power performance of cathodes affected by biofouling, *Appl. Energy* 173 (2016) <https://doi.org/10.1016/j.apenergy.2016.04.009>.
- [48] W. Yang, R. Rossi, Y. Tian, K.-Y. Kim, B.E. Logan, Mitigating external and internal cathode fouling using a polymer bonded separator in microbial fuel cells, *Bioresour. Technol.* (2017) 0–1, <https://doi.org/10.1016/j.biortech.2017.10.109>.
- [49] M. Santini, S. Marzorati, S. Fest-Santini, S. Trasatti, P. Cristiani, Carbonate scale deactivating the biocathode in a microbial fuel cell, *J. Power Sources* 356 (2017) 400–407, <https://doi.org/10.1016/j.jpowsour.2017.02.088>.
- [50] J. Xu, G.-P. Sheng, H.-W. Luo, W.-W. Li, L.-F. Wang, H.-Q. Yu, Fouling of proton exchange membrane (PEM) deteriorates the performance of microbial fuel cell, *Water Res.* 46 (2012) 1817–1824, <https://doi.org/10.1016/j.watres.2011.12.060>.

- [51] M. Miskan, M. Ismail, M. Ghasemi, J. Md Jahim, D. Nordin, M.H. Abu Bakar, Characterization of membrane biofouling and its effect on the performance of microbial fuel cell, *Int. J. Hydrog. Energy* 41 (2016) 543–552, <https://doi.org/10.1016/j.ijhydene.2015.09.037>.
- [52] J. An, N. Li, L. Wan, L. Zhou, Q. Du, T. Li, X. Wang, Electric field induced salt precipitation into activated carbon air-cathode causes power decay in microbial fuel cells, *Water Res.* 123 (2017) 369–377, <https://doi.org/10.1016/j.watres.2017.06.087>.
- [53] L. Zhang, X. Zhu, J. Li, Q. Liao, D. Ye, Biofilm formation and electricity generation of a microbial fuel cell started up under different external resistances, *J. Power Sources* 196 (2011) 6029–6035, <https://doi.org/10.1016/j.jpowsour.2011.04.013>.
- [54] T. Mumtaz, M.R. Khan, M.A. Hassan, Study of environmental biodegradation of LDPE films in soil using optical and scanning electron microscopy, *Micron* 41 (2010) 430–438, <https://doi.org/10.1016/j.micron.2010.02.008>.
- [55] K. Shang, J. Rnjak-Kovacina, Y. Lin, R.S. Hayden, H. Tao, D.L. Kaplan, Accelerated in vitro degradation of optically clear low β -sheet silk films by enzyme-mediated pretreatment, *Transl. Vis. Sci. Technol.* 2 (2013) 2, <https://doi.org/10.1167/tvst.2.3.2>.
- [56] Y. Cao, B. Wang, Biodegradation of silk biomaterials, *Int. J. Mol. Sci.* 10 (2009) 1514–1524, <https://doi.org/10.3390/ijms10041514>.